IEEE Access
Multidisciplinary | Rapid Review | Open Access Journal

Received 28 November 2023, accepted 31 December 2023, date of publication 8 January 2024,
date of current version 17 January 2024.

*Digital Object Identifier 10.1109/ACCESS.2024.3351475*

RESEARCH ARTICLE

# A Miniaturized Metamaterial-Loaded Switched-Beam Antenna Array System With Enhanced Bandwidth for 5G Applications

**ARSHAD KARIMBU VALLAPPIL[1], MOHAMAD KAMAL A. RAHIM[2], (Senior Member, IEEE), BILAL A. KHAWAJA[3], (Senior Member, IEEE), AND MUHAMMAD NAEEM IQBAL[2]**

[1]Institute of Space Sciences (ICE-CSIC), Campus UAB, 08193 Barcelona, Spain
[2]Advance RF and Microwave Research Group (ARFMRG), Faculty of Electrical Engineering, Universiti Teknologi Malaysia (UTM), Johor Bahru, Johor 81310, Malaysia
[3]Faculty of Engineering, Department of Electrical Engineering, Islamic University of Madinah, Madinah 41411, Saudi Arabia

Corresponding authors: Arshad Karimbu Vallappil (karimbu@ice.csic.es) and Mohamad Kamal A. Rahim (mdkamal@utm.my)

This work was supported by the Ministry of Higher Education (MOHE) under Fundamental Research Grant Scheme FRGS/1/2021/STG04/UTM/01/1 and grant 09G19 School of Postgraduate Studies (SPS), Research Management Centre, Advanced RF and Microwave Research Group, Faculty of Electrical Engineering, Universiti Teknologi Malaysia (UTM), Johor Bahru.

**ABSTRACT** In this research study, a metamaterial (MTM) based $1 \times 4$ linear antenna array is designed with an integrated butler matrix (BM) beamforming network (BFN) to execute the switched-beam antenna array (SAA) operation, which can be employed for sub-6 GHz 5G applications. The proposed SAA is designed and simulated using CST microwave studio and then fabricated using FR4 epoxy glass substrate with the thickness $(h) = 1.6$mm and dielectric constant $(\varepsilon_r) = 4.3$. The MTM-BM BFN has shown excellent performance in both simulated and measured results, having return-loss of below 14 dB and insertion-loss at ports 5-8 to be $7 \pm 2$dB between the frequency range of 3.2-3.75GHz, respectively. Moreover, the phase difference between the output ports of the BM is simulated and measured. The $0.5\lambda$ spaced complementary split-ring resonator (CSRR) based antenna array integrated with MTM-BM BFN achieved a measured gain of 4.8-6.1 dB when each input port of BM was excited. The SAA analysis has been performed to identify the variation of gain and grating lobes; the distance between MTM antennas was altered by $0.3\lambda$, $0.5\lambda$, and $0.7\lambda$, respectively. Depending on the BM input ports excitation, the main beam of the SAA is steered in four different directions $-40°$, $-15°$, $+15°$, and $+45°$, respectively. These radiation pattern studies have shown that the MTM-BM connected with four linear MTM antennas has successfully generated four beams in four different directions, which can be utilized for 5G applications to improve the channel capacity and enhance the transmission quality.

**INDEX TERMS** 5G, metamaterial (MTM), antenna array, Butler matrix (BM), beamforming network (BFN), switched-beam antenna array (SAA), complementary split-ring resonator (CSRR).

## I. INTRODUCTION

In today's modern world, the ever-growing demand for reliable and high-speed wireless technology is exponentially increasing because of the huge data traffic from different channels like social media applications, cloud computing platforms, live streaming websites, artificial intelligence (AI) applications, virtual reality, and online gaming, etc [1], [2], [3]. Currently, ~23-billion wireless devices and sensors are linked to the internet network, and in the future, these numbers are expected to rise manifold [1], [2], [3]. In order to meet these demands, researchers and technology companies are

The associate editor coordinating the review of this manuscript and approving it for publication was Guido Valerio.

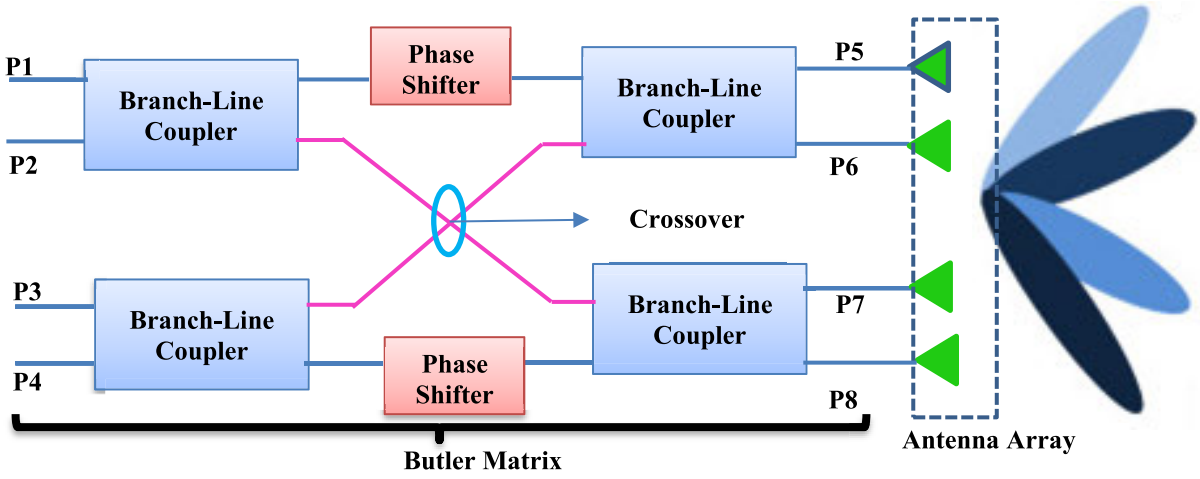


**FIGURE 1.** Switched-beam antenna array.

putting tremendous effort into the development and deployment of Fifth Generation (5G) wireless technology [1], [2], [3]. These 5G wireless systems are anticipated to provide ∼10GB/s data-rates, extremely low wireless signal latency, increased bandwidth for higher user capacity of up to several billion, and reduced power consumption. Another significant aspect of the 5G wireless systems is the utilization of sub-6GHz and millimeter-wave (mm-Wave) frequency bands [2], [3], [4], [5], [6].

Long ago [7], when the researchers started to explore the possibilities for 5G wireless systems as a next-generation wireless standard, they predicted that antenna arrays with beam-switching capabilities would be required for the signal distribution in the upcoming wireless technology [8], [9]. For this purpose, it was envisioned that beam-forming networks (BFNs) based on switched-beam antenna array (SAA) technology could play a critical role in solving design constraints like multi-path fading and interference, which affects the overall quality of the transmitted wireless signal [10].

The SAA technology mainly comprises antenna arrays and BFNs, where the predefined phases from the BFN can be utilized to steer the main beam of the antenna array in any desired direction. So, the above-mentioned problems can be solved by employing multiple antenna elements integrated with BFNs (an SAA system) at the 5G transceivers to improve the overall directionality, coverage, and resolution along the desired 5G signal path [2], [10]. It is also important to note that since the 5G wireless systems provide an enhanced bandwidth of 0.5-1GHz compared to previous wireless generations, the compact structure of the SAA system is a critical design requirement [11].

For the upcoming 5G wireless systems, it is significant to define the optimal method for deploying BFNs, which leads researchers to study the design and performance trade-offs between the existing SAA technologies. Typically, the BFNs are mainly divided into two major categories of analog and digital BFNs [12]. Then, the analog BFNs are further divided into two sub-categories which are variable phase-shifter (VPS) and fixed-passive BFN [13]. The VPS BFNs are even further sub-classified into active and passive VPSs. Some of the noteworthy drawbacks of the active and passive VPSs are high insertion-loss and power consumption, respectively [13]. Typically, the fixed-passive BFNs refer to the lens- or circuit-based BFN. Butler matrix (BM) [14] is considered one of the most commonly used and preferred circuit-based BFNs. So, in this paper, we will focus our discussion on the metamaterial (MTM) structure based SAAs to meet the requirements of the upcoming 5G system with excellent performance characteristics. MTMs [15], [16], [17] are typically defined as artificially constructed materials which can attain negative magnetic permeability ($\mu$) and electric permittivity ($\varepsilon$). The negative $\mu$ and $\varepsilon$ properties for the microwave components offer benefits like electrically small size, high bandwidth, and good performance characteristics for the future 5G systems.

In this research study, all components of the SAA system are designed based on the MTM transmission-line (MTM-TL) technique consisting of a 4 × 4 BM (including BLC and crossover) as well as an antenna designed on a single FR4 substrate sharing a common ground plane to meet the requirements of 5G systems [11].

In 5G SAA systems, the proposed MTM-BM has to feed the signal to the MTM antenna array. Thus, the SAA radiates signals at 5G frequency bands in four different predefined directions due to the progressive phase difference between the BM output ports. Ultimately, this proposed SAA system generates beams in four different directions, which will help reduce co-channel interference and multipath fading in 5G wireless systems. This leads to improve the channel capacity and enhances the transmission quality [18].

## II. DESIGN AND CHARACTERIZATION OF BEAMFORMING NETWORK FOR SWITCHED-BEAM ANTENNA ARRAY (SAA)

The proposed SAA is constructed by a linear antenna array of four radiating elements using the FR4 substrate and the BFN. The desired radiation main beam is selected by the

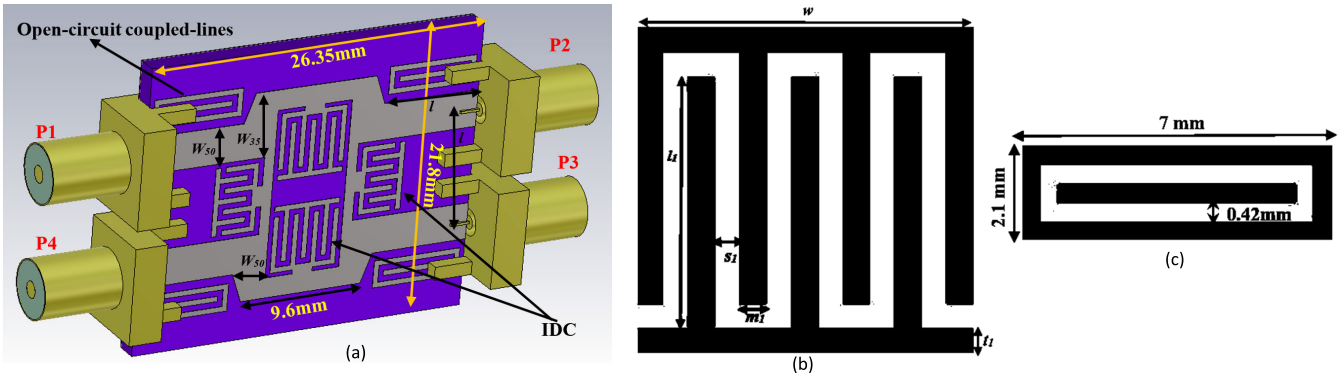


**FIGURE 2.** (a) Proposed configuration of MTM based BLC (b) IDC (c) Open-circuit coupled-lines.

BFN. This analog BFN is the 4 × 4 BM with 4 outputs ports (P5, P6, P7, and P8) connected to four antennas. The novelty of this research is that all the components of SAA is constructed by using MTM-TL. The open coupled-lines and inter-digital capacitor (IDC) unit-cell are used in this design to achieve MTM-TL properties. Fig. 1 shows the proposed SAA structure.

BM is one of the BFNs for use in the SAA system. By using BM, various beams in different directions can be easily produced. With an adaptive control unit in the antenna system, those beams can be used to provide a fast discrete electronic scanning of the antenna pattern [19]. BM is an $N \times N$ network consisting of $N$ inputs and $N$ outputs. The total number of ports is $2N$. Orthogonal beams pointed at different angles can be generated in the SAA system by connecting $N \times N$ BM to the $N$-elements array antenna [19].

As illustrated in Fig. 1, the construction of the standard BM is composed of three main components; 3-dB couplers, crossovers, and 45° phase shifters. In BM design, one of the important specifications is the phase difference between the radiating elements. Based on the design principle introduced by Moody [20], for $N$-elements BM, the phase difference between the radiating elements can be calculated by using Eq. (1).

$$Phase\ difference = \pm\left(\frac{2i-1}{N}\right)\pi \tag{1}$$

where, $N$ is the matrix order, and $i$ is the number of the input port. As an example, for 4 × 4 BM, when the signal was excited into Port-1, the value of $i$ is equal to 1, and the $N$ can be substituted to 4. Therefore, when substituting the values of $i$ from 1 to 4, the phase differences for output from input Port-1 and Port-4 are ±45°; meanwhile, the phase differences for output from input Port-2 and Port-3 are ±135°.

From Fig. 1, it can be observed that with different excitation of the input port, different beam directions will be formed at the output ports with constant phases of −45°, +135°, −135°, and +45° [21], [22]. For example, when Port-1 (P1) of BM is fed with signal, a phase difference of −45° is obtained between P6 and P5, P7 and P6, and P8 and P7. Meanwhile, when P2, P3, and P4 are excited with signal, phase differences of −135°, +135°, and +45° are obtained, respectively.

**TABLE 1.** Dimensions of MTM BLC.

| Description | Notation | Dimension (mm) |
|---|---|---|
| **BLC Arm** | | |
| Width of 50Ω Impedance line | $W_{50}$ | 2.8 |
| Width of 35Ω Impedance line | $W_{35}$ | 5 |
| Length of the feed line | $l$ | 8.7 |
| HORIZONTAL ARM | | |
| Finger Width | $m_1$ | 0.4 |
| Finger Length | $l_1$ | 3.9 |
| Width of IDC | $w$ | 5.2 |
| Finger Gap | $s_1$ | 0.4 |
| Exterior Finger Width | $t_1$ | 0.4 |
| VERTICAL ARM | | |
| Finger Width | $m_1$ | 0.4 |
| Finger Length | $l_1$ | 2.2 |
| Width of IDC | $w$ | 5.2 |
| Finger Gap | $s_1$ | 0.4 |
| Exterior Finger Width | $t_1$ | 0.4 |

Another important parameter of BM is the insertion-loss. The theoretical insertion-loss between Port-1 (P1) and output ports (P5–P8) should be 6 dB, respectively. This indicates that the BM circuit divides the transmitted input power to approximately four signals. Similarly, the insertion-loss between P2/P3/P4 and output ports (P5-P8) should be 6 dB. But in practice, it is not possible due to several number components in BM. In this research, the insertion-loss of 7±1.5dB and phase difference of ±45 and ±135 can be achieved between consecutive output ports by exciting one of the input ports. The open coupled-lines and IDC unit-cell that develops MTM properties are applied to the components of modified 4 × 4 BM in order to achieve miniaturization and enhance bandwidth performance in this research work. All the components of BM are designed using FR4 substrate ($\varepsilon_r = 4.3$ and $h =$ 1.66 mm) and operate at the center frequency of 3.5GHz, having a bandwidth of 500MHz. In the next sub-section, the design of all components of MTM-BM and SAA are discussed in a detailed manner.

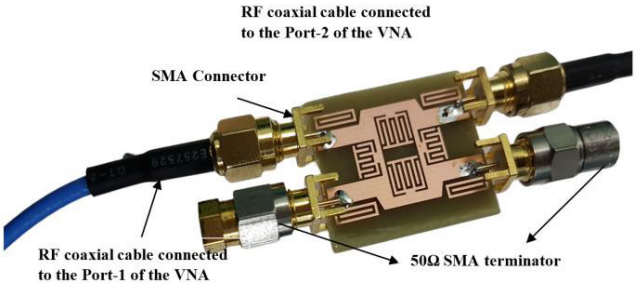


**FIGURE 3.** Fabricated prototype of MTM based BLC.

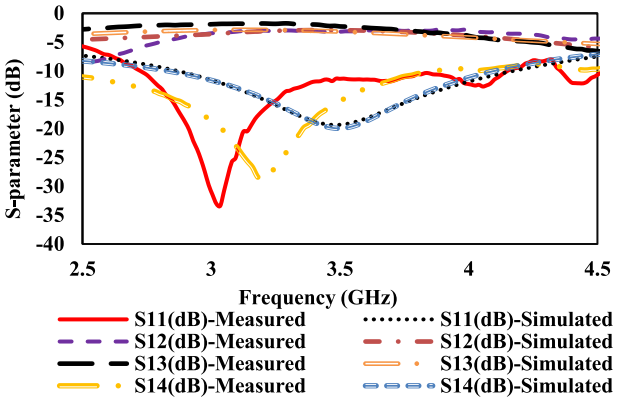


**FIGURE 4.** S-parameter response of proposed designed and fabricate BLC (both simulated and measured response).

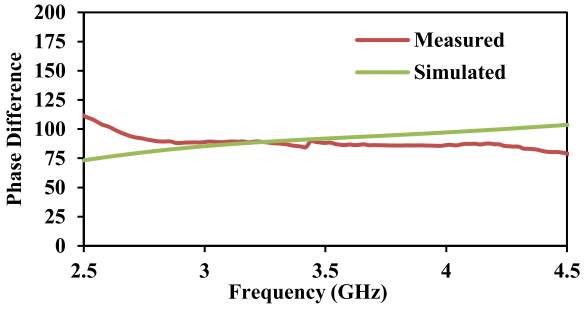


**FIGURE 5.** Simulated and measured phase difference between Port-2 and Port-3.

### A. DESIGN OF MTM BASED BRANCH-LINE COUPLER (BLC)

The proposed design of MTM based BLC is shown in Fig. 2 (a-c). As shown in Fig. 2(a), the BLC consists of two input ports and two output ports [23]. The input and output ports are labeled as P1, P4, and P2, P3, respectively. Theoretically, the couplers were designed to have −3dB insertion-loss, with a phase difference between the output ports P2 and P3 being 90° [23].

BLC's horizontal and vertical TL impedances are $Z_0/\sqrt{2}$ and $Z_0$, respectively. The $Z_0$ in the designed BLC is set to 50Ω. The length of the line impedance at each branch is $\lambda/4$. Fig. 2(b) depicts the IDC unit-cell employed in the BLC's vertical arm. Equations [24] can be used to calculate the BLC's width ($W$) and feed length ($l$). The substrate has

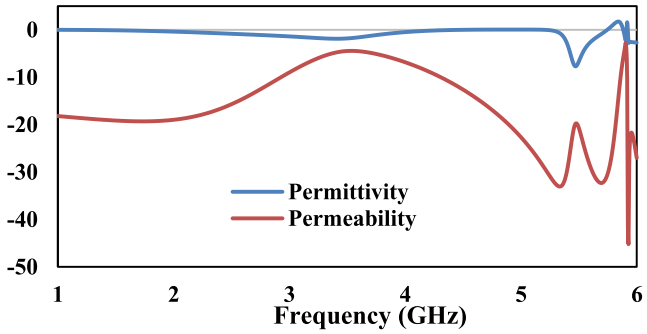


**FIGURE 6.** Permeability and permittivity properties of MTM based BLC.

been selected as FR4 with $\varepsilon_r$ and thickness ($h$) of 4.3 and 1.6mm, respectively.

To attain MTM features, the proposed BLC has been incorporated with four open-circuits coupled-lines at each port and an IDC at the horizontal and vertical arms of the transmission line (TL), as shown in Fig. 2. The loading of open-circuit coupled-lines at each port of the proposed BLC improves the bandwidth. The dimensions of the proposed BLC are shown in Table 1.

The fabricated prototype of the proposed MTM based BLC is shown in Fig. 3. The simulated and measured S-Parameter performance of the proposed BLC is shown in Fig. 4. The results show that the proposed BLC was operating between the frequency range of 2.87GHz to 4.17GHz with a coupling factor ($S_{12}$ and $S_{13}$) of 3±1dB. Fig. 5 illustrates the phase difference between output ports of BLC. The proposed BLC achieved a phase difference of 88° at 3.5GHz and 90° ± 5° between 2.87GHz to 4.17GHz. As compared to the theoretical value, the phase-error was 2° at 3.5GHz.

The MTM-TL properties of BLC are calculated by using Nicolson Ross Weir (NRW) method [25]. NRW is a methodology used to obtain the $\varepsilon$ and the $\mu$ from the S-parameters. The material with negative $\varepsilon$ and $\mu$ simultaneously in certain frequency ranges is called left-handed MTMs (LH-MTMs). The NRW method obtains the $\varepsilon$ and $\mu$ using the following constants:

So, writing the sums and differences of the scattering coefficients as:

$$V_1 = S_{21} + S_{11} \tag{2}$$

$$V_2 = S_{21} - S_{11} \tag{3}$$

$$X = \frac{1 - V_1 V_2}{V_1 - V_2} \tag{4}$$

Then it can be shown that $\mathbb{\Gamma}$ may be obtained from the scattering coefficients, since:

$$\Gamma = X \pm \sqrt{X^2 - 1} \tag{5}$$

and the appropriate sign is chosen so that $\acute{\Gamma} < 1$. Also,

$$z = \frac{V_1 - \Gamma}{1 - V_1 \Gamma} \tag{6}$$

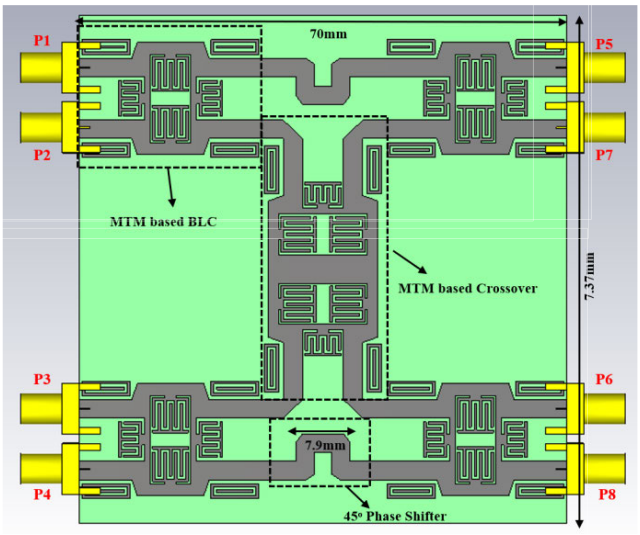


**FIGURE 7.** The proposed layout of the MTM-BM.

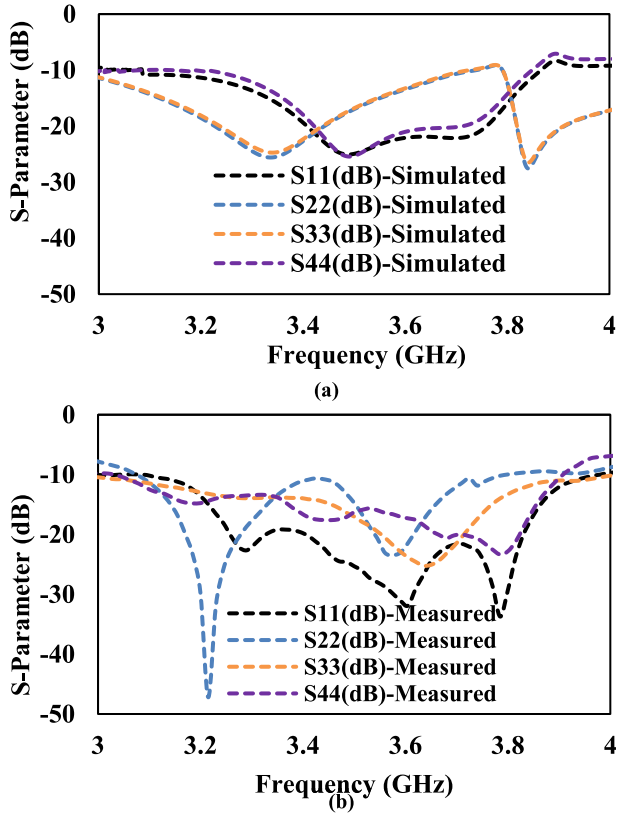


**FIGURE 8.** The proposed layout of the MTM-BM S-parameters results in terms of return-loss (a) Simulated and (b) measured.

$$\frac{\mu_r}{\varepsilon_r} = \left(\frac{1+\Gamma}{1-\Gamma}\right)^2 = c_1 \tag{7}$$

$$\mu_r \varepsilon_r = -\left\{\frac{c}{\omega d} ln\left(\frac{1}{z}\right)\right\}^2 = c_2 \tag{8}$$

Then,

$$\mu_r = \sqrt{c_1 c_2} \tag{9}$$

**TABLE 2.** Summary of the proposed 4 × 4 butler matrix S-parameter response at 3.5GHz.

| Output Port | S-Parameter | Simulation (dB) | Measured (dB) | Desired Value (dB) |
|---|---|---|---|---|
| Port-5 | $S_{15}$ | -7.2 | -7.5 | -7 ± 2 |
| | $S_{25}$ | -5.8 | -7.1 | |
| | $S_{35}$ | -6.1 | -8.3 | |
| | $S_{45}$ | -5.6 | -7.2 | |
| Port-6 | $S_{16}$ | -6.1 | -7.5 | -7 ± 2 |
| | $S_{26}$ | -5 | -6.2 | |
| | $S_{36}$ | -5.6 | -8.4 | |
| | $S_{46}$ | 5.9 | -5.6 | |
| Port-7 | $S_{17}$ | -5.85 | -7.2 | -7 ± 2 |
| | $S_{27}$ | -5.6 | -8 | |
| | $S_{37}$ | -5 | -7.5 | |
| | $S_{47}$ | -6.1 | -6.7 | |
| Port-8 | $S_{18}$ | -5.6 | -5.8 | -7 ± 2 |
| | $S_{28}$ | -6.1 | -6.8 | |
| | $S_{38}$ | -5.85 | -6.7 | |
| | $S_{48}$ | -7.2 | -7.5 | |

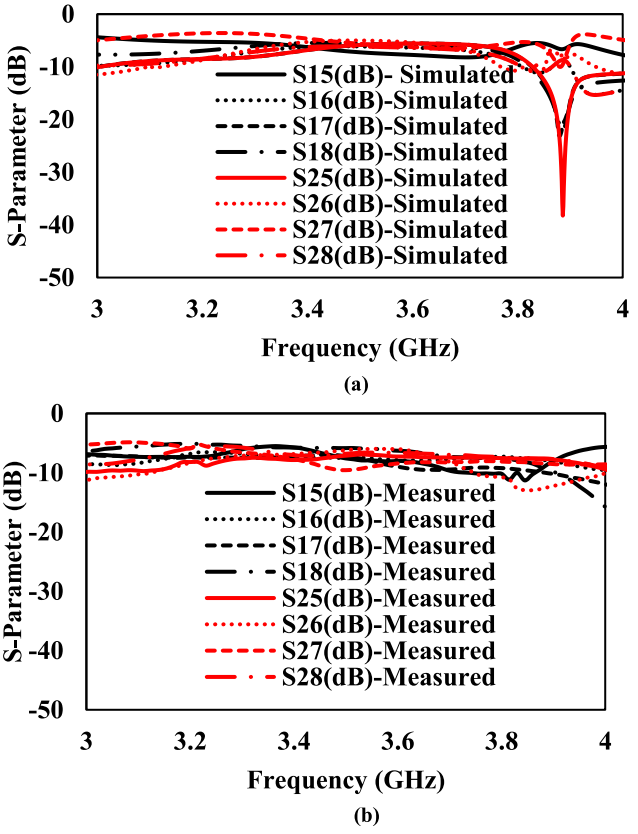


**FIGURE 9.** Insertion-loss response for the Port-1 and Port-2 excitation (a) Simulated (b) Measured.

$$\varepsilon_r = \sqrt{\frac{c_2}{c_1}} \tag{10}$$

Fig. 6 depicts that the $\mu$ and $\varepsilon$ are obtained from the measurement of the transmission and reflection scattering

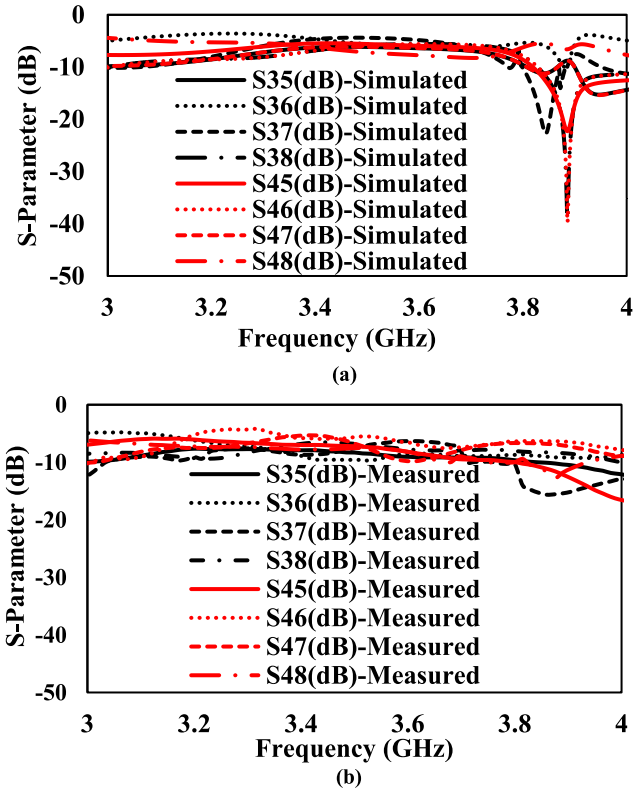


**FIGURE 10.** Insertion-loss response for the Port-1 and Port-2 excitation (a) Simulated (b) Measured.

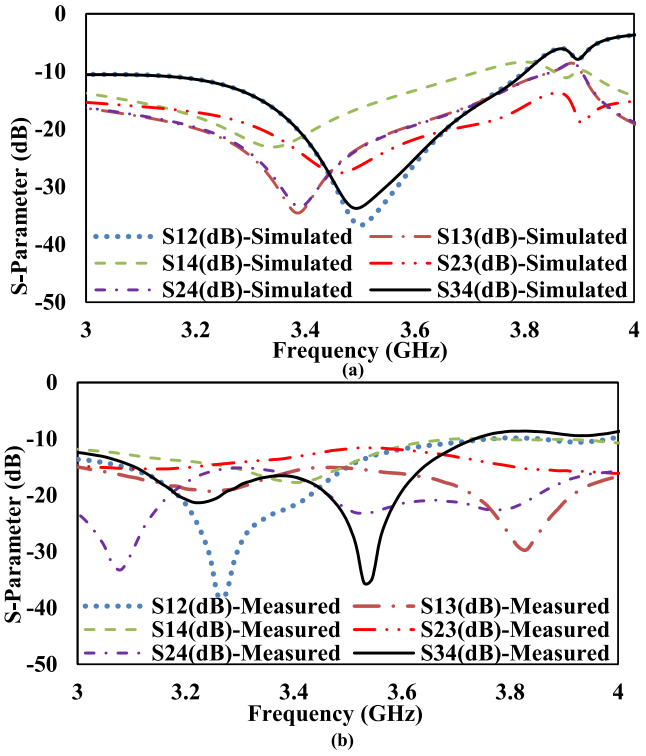


**FIGURE 11.** Isolation-loss response (a) Simulated and (b) Measured.

coefficients of a MTM based BLC. From Fig. 6, it is understood that the value of $\varepsilon$ and $\mu$ is negative between the frequency ranges of 1.8GHz to 5.1GHz. This proves that the proposed BLC shows MTM-TL properties due to the negative value of $\varepsilon$ and $\mu$ simultaneously for a certain frequency range.

The next component of BM is the crossover, and it was implemented by cascading two MTM based BLCs presented in the above section.

### B. DESIGN OF MTM-BASED BM

The BM consists of 4 BLCs of 90° phase difference between the output ports, two phase-shifters that provide a phase shift of 45°, and a crossover to avoid the overlapping of signals at the crossing. As shown in Fig. 7, the input ports are represented as P1, P2, P3, and P4, and the output ports are indicated as P5, P6, P7, and P8. The proposed layout of the new BM is shown in Fig. 7. In designing a BM, four parameters are considered; phase difference between output ports, insertion-loss, return-loss, and isolation-loss. Insertion-loss defines how the input power is split between the output ports. The proposed BM was validated in accordance with the design criteria discussed in detail in Section II.

Fig. 8(a-b) discusses the simulated and measured S-parameters results in terms of return-loss. For the simulation and measurement setup of $S_{11}$, P1 is fed with the signal while keeping all the other terminated using 50Ω loads. A similar procedure has been repeated for $S_{22}$, $S_{33}$, and $S_{44}$. The results are summarized in Fig. 8(a-b), and it can be observed that the simulated and measured return-loss is coming out to be below 10dB between the frequency range 3.1GHz- 3.8GHz.

Fig. 9(a-b) discusses the simulated and measured S-parameters results in terms of insertion-loss for P1 and P2 excitation. From 3.2GHz to 3.75GHz frequency range, the results in Fig. 9(a-b) illustrate that the simulated and measured insertion-loss obtained at P5-P8 is $7 \pm 2$dB. According to the insertion-loss result observed in Fig. 9(a-b), the power division between the BM four output ports is approximately equal.

Fig.10 (a-b) discusses the simulated and measured S-parameters results in terms of insertion-loss for P3 and P4 excitation. The results are summarized in Fig. 10(a-b). It can be observed that simulated and measured insertion-loss at P5-P8 is coming out to be $7 \pm 2$dB, respectively which shows that output ports power division in the BM network is approximately equal. All the simulated and measured responses are taken between the frequency range of 3.2-3.75GHz, respectively. The summary of the proposed $4 \times 4$ Butler Matrix S-Parameter Response at 3.5GHz is shown in Table 2.

Fig. 11(a-b) illustrates the simulated and measured response of the isolation-loss at the input ports. From 3GHz to 3.8GHz frequency range, the results in Fig. 11(a-b) indicate that the measured and simulated isolation-loss is below 10dB. So, this shows excellent isolation between the input ports. There is a shift in the resonance points of measured and simulated S-Parameter results value which is due to the

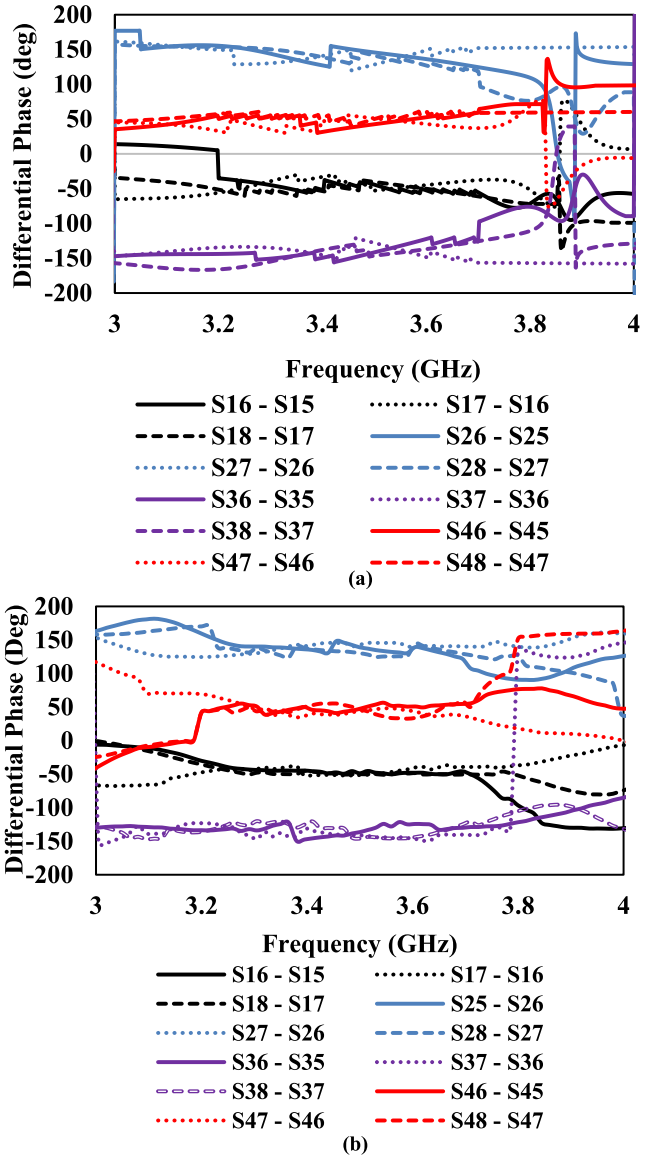


**FIGURE 12.** Phase difference between the adjacent output ports of the BM when P1, P2, P3, and P4 are excited (a) Simulated (b) Measured.

variations in the lossy FR4 substrate properties (loss-tangent ($tan\delta$) = 0.025) and the amount of solder. This discrepancy can be improved by using high-end Roger's substrates with low loss tangent value.

This paragraph summarizes the phase difference characteristics between adjacent output ports of the BM. The phase difference is calculated by subtracting the phase from one output port to another. Fig. 12(a-b) shows the simulated and measured phase difference between the adjacent output ports of the BM when P1, P2, P3, and P4 are excited. Results in Fig. 12(a-b) show good agreement between the simulated and measured phase differences.

So, for the Port-1 excitation of the proposed BM design at 3.5GHz, the simulated and measured phase differences ($S_{16}$-$S_{15}$) / ($S_{17}$-$S_{16}$) / ($S_{18}$-$S_{17}$) of −44.2°/−52.8°/ −40.3° and −42.7°/ −51.4°/−54° is achieved between P5 / P6, between P6 / P7 and between P7 / P8, respectively. The ideal phase difference between the output ports for P1 excitation is −45° as per Eq. 1. It can be noted from the simulated phase difference values that the errors are 0.8°, 7.8°, and 4.7°, respectively. The average phase difference error is 4.4°. It is important to note here that from the measured phase difference values, the error is 2.3°, 6.4°, and 9°, respectively. Similarly, for the excitation of P2, P3, and P4, the simulated and measured phase difference between the adjacent output ports results are summarized in Table 3.

**TABLE 3.** Proposed 4 × 4 BM simulated and measured phase difference between the output ports at 3.5 GHz.

| Phase difference between consecutive ports | | Simulated (Degrees) | Measured (Degrees) | Expected Value (Degrees) |
|---|---|---|---|---|
| Port-1 | Phase ($S_{16}$)- Phase ($S_{15}$) | -44.2 | -42.7 | -45° |
| | Phase ($S_{17}$)- Phase ($S_{16}$) | -52.8 | -51.4 | |
| | Phase ($S_{18}$)- Phase ($S_{17}$) | -40.3 | -54 | |
| Port-2 | Phase ($S_{26}$)- Phase ($S_{25}$) | 145 | 139 | 135° |
| | Phase ($S_{27}$)- Phase ($S_{26}$) | 129 | 142 | |
| | Phase ($S_{28}$)- Phase ($S_{27}$) | 141 | 130.3 | |
| Port- 3 | Phase ($S_{36}$)- Phase ($S_{35}$) | -141.6 | -136.5 | -135° |
| | Phase ($S_{37}$)- Phase ($S_{36}$) | -128 | -141 | |
| | Phase ($S_{38}$)- Phase ($S_{37}$) | -146.5 | -146 | |
| Port- 4 | Phase ($S_{46}$)- Phase ($S_{45}$) | 42.6 | 47.4 | 45° |
| | Phase ($S_{47}$)- Phase ($S_{46}$) | 51 | 44 | |
| | Phase ($S_{48}$)- Phase ($S_{47}$) | 50 | 46.8 | |

In Section II-B, an MTM based 4 × 4 BM was designed, simulated, and fabricated for the 5G SAA system. The proposed 4 × 4 BM was designed using IDC and open-circuit coupled-lines to achieve MTM-TL properties. Four parameters that include return-loss, isolation-loss, insertion-loss, and phase difference results have been addressed for the proposed BM. The proposed BM has shown excellent performance in simulated and measured results, with return-loss and isolation-loss values to be below −14dB, insertion-loss at ports 5-8 to be 7 ± 2dB between the frequency range of 3.2-3.75GHz, respectively. Further evidence shows that the size of the proposed BM decreased by 75% (Size = 70mm × 73.7mm), and the bandwidth (550MHz) was enhanced about 8.2 times higher than the traditional BM [19].

## III. INTEGRATION AND CHARACTERIZATION OF SAA

In this section, a SAA based on MTM-BM is designed for 5G applications. A MTM antenna array connected with MTM-BM was presented to develop SAA, as shown previously in Fig.1. The use of BM is to shift the beam in a different direction. The proposed BM in section II-B, develops a −45°, +135°, −135°, and +45° phase difference between the

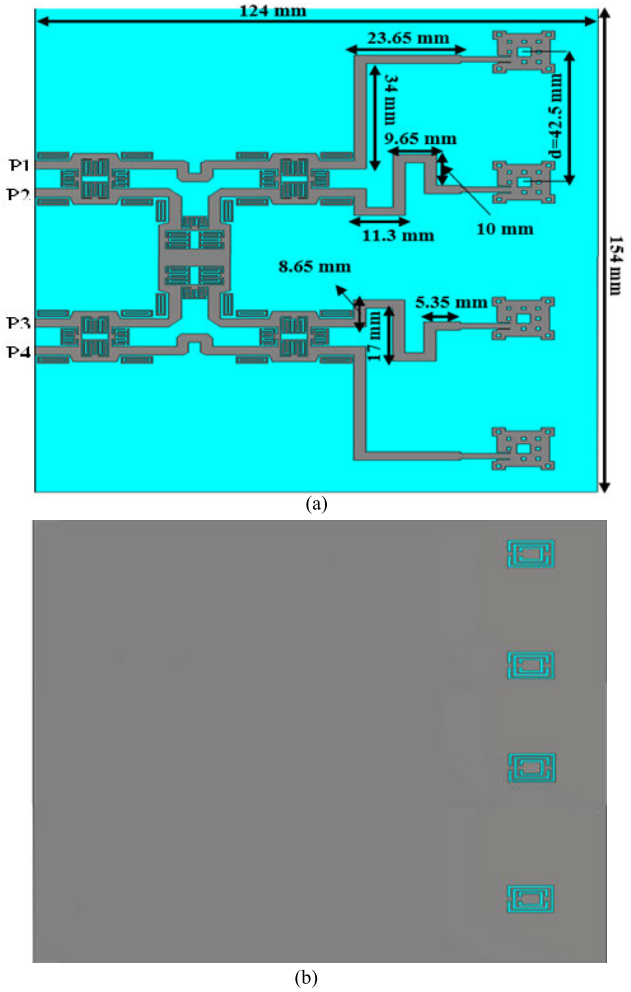


**FIGURE 13.** Layout MTM based BM connected to linear MTM antenna array with spacing d = 0.5$\lambda$ (a) Top Layer (b) Bottom Layer.

output ports with a maximum average phase tolerance of $\pm 5°$ at 3.5GHz based on the excitation of the input ports. Therefore, it is possible to direct the main beam to $\pm 15°$ and $\pm 45°$ by connecting four MTM antennas presented in [15] with a half-wavelength distance [18] and feed the antenna using MTM based BM. The beam of SAA in Fig.1 may also be directed to a particular angular direction by controlling the phase difference between the output ports of BM and the distance between the antenna elements. This work aims to develop a beam-steering array antenna with an emphasis on the radiation pattern. In the following section, the overall design is further elaborated.

### *A. LINEAR ANTENNA ARRAY (1 × 4) WITH METAMATERIAL BUTLER MATRIX*

A linear antenna array of four MTM antennae based on a combined Minkowski-Sierpinski carpet fractal antenna (CMSFA) radiating patch with CSRR etched in the ground plane and the BFN was used to construct the SAA. The substrate chosen was an FR4 with a relative permittivity ($\varepsilon_r$) of 4.3 and a thickness ($h$) of 1.6mm, respectively. The BFN and

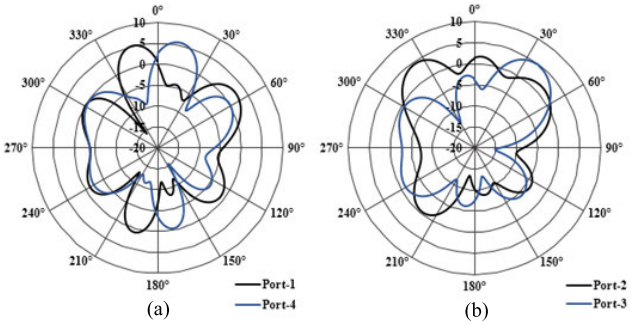


**FIGURE 14.** Simulated radiation pattern results of 1×4 antenna array with a spacing of 0.5$\lambda$ (a) Port-1 or Port-4 are excited (b) Port-2 or Port-3 are excited.

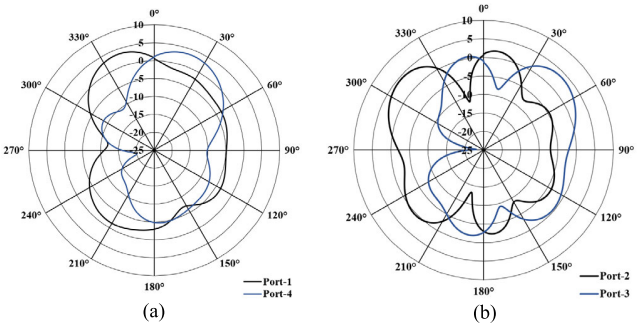


**FIGURE 15.** Simulated radiation pattern results of 1×4 antenna array with a spacing of 0.3$\lambda$ (a) Port-1 or Port-4 are excited (b) Port-2 or Port-3 are excited.

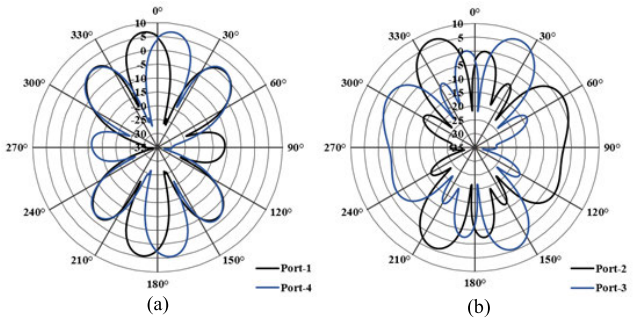


**FIGURE 16.** Simulated radiation pattern results of 1×4 antenna array with a spacing of 0.7$\lambda$ (a) Port-1 or Port-4 are excited (b) Port-2 or Port-3 are excited.

distance between the antenna elements select the direction of the main beam radiation. The BFN is the 4 × 4 BM presented in section II-B, and it has four output ports (P5, P6, P7, and P8) connected to the MTM antenna, as shown in Fig. 13. More information and detailed step-by-step design of the MTM antenna is presented in [15]. The MTM antenna radiating patch is based on the fractal structure of the combined Minkowski-Sierpinski carpet, and complementary split-ring resonator (CSRR) structures are etched in the ground plane to miniaturize the antenna size and improve the antenna's overall bandwidth. Initially, the spacing between the antenna elements was adjusted to half-wavelength, which is about

**TABLE 4. Comparison of the simulated pattern results and the gain according to the spacing between the antenna elements (*d*).**

| Port | Gain (dB) | | | Main beam direction | | |
|---|---|---|---|---|---|---|
| | $d = 0.3\lambda$ | $d = 0.5\lambda$ | $d = 0.7\lambda$ | $d = 0.3\lambda$ | $d = 0.5\lambda$ | $d = 0.7\lambda$ |
| Port-1 | 3.63 | 5.23 | 6.4 | -25° | -15° | -8° |
| Port-2 | 4.33 | 4.4 | 6.5 | -50° | -40° | -23° |
| Port-3 | 3.68 | 5.1 | 6.6 | +50° | +40° | +23° |
| Port-4 | 3.52 | 5.77 | 6.4 | +25° | +15° | +8° |

42.5mm. The overall dimension of the structure is 124 × 154 mm$^2$. Secondly, the spacing between the MTM antenna is updated by $d = 0.3\lambda$ and $d = 0.7\lambda$. The main purpose of updating the spacing '$d$' is to identify the variation in main beam angles and grating lobe to achieve better gain. The relationship between the main beam angle $\theta$ of the antenna array and the phase difference between two continuous elements in the array ($\beta$) are given in Eq. 11:

$$\Psi = (kd\ cos\theta + \beta) \tag{11}$$

The simulated radiation pattern results of the linear 1 × 4 antenna array with spacing $0.5\lambda$ are shown in Fig. 14(a) when P1 or P4 of the BM is excited. Fig. 14(b) shows the simulated results of the radiation pattern, when P2 or P3 of the BM is excited. Firstly, we are discussing the simulation results for $d = 0.5\lambda$ at 3.5GHz. When P1 and P4 are excited, a gain of 5.23dB and 5.77dB is achieved, respectively. Although the gain decreases to 4.4dB and 5.1dB for P2 and P3 excitation, respectively. However, according to which input port is excited, the peak of the beam rotates.

As seen in Fig. 14(a), when input port P1 is fed with a signal, the main beam is directed to −15°. Meanwhile, the direction of maximum radiation is attained at −40° as the signal is fed into input port P2. In Fig. 14(b), for the input port P3 excitation, the main beam steers to +40°. When the input port P4 is excited, the direction of the main beam alters to +15°. In the case of $d = 0.5\lambda$, when the input port P1 and P4 are excited, the half-power beam-width (HPBW) of the main lobe is 22.3° and 23.6°, respectively. Similarly, the HPBW is 31.7° and 33.7° for the excitation of input ports P2 and P3, respectively.

Secondly, we are discussing the simulation results for $d = 0.3\lambda$ at 3.5GHz. A gain value of 3.63dB, 4.33dB, 3.68dB, and 3.52dB was achieved when P1, P2, P3, and P4 were excited, respectively. In Fig. 15(a), when input ports P1 and P4 were excited, the main beam direction was achieved at −25° and +25°, respectively. As seen in Fig. 15(b), as input ports P2 and P3 were fed with signal, the direction of maximum radiation was attained at −50° and +50°, respectively. In the case of $d = 0.3\lambda$, when the input ports P1 and P4 are excited, the HPBW of the main lobe is 44.7° and 49.6°, respectively. Similarly, the HPBW is 43° and 44.6° for the excitation of input ports P2 and P3, respectively.

Finally, we are discussing simulation results for $d = 0.7\lambda$ at 3.5GHz. A gain of 6.4dB, 6.5dB, 6.6dB, and 6.4dB was

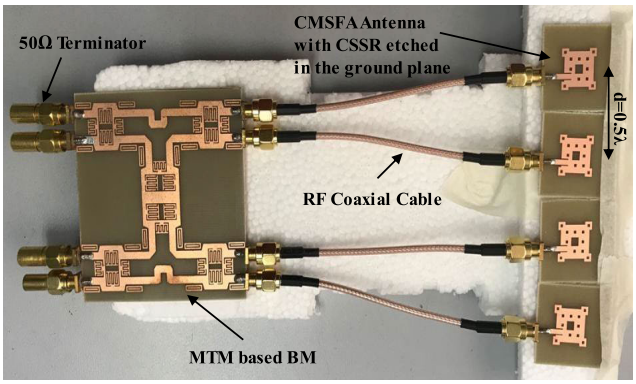


**FIGURE 17. Hybrid implementation of the SAA and the spacing between the antenna elements d = 0.5$\lambda$.**

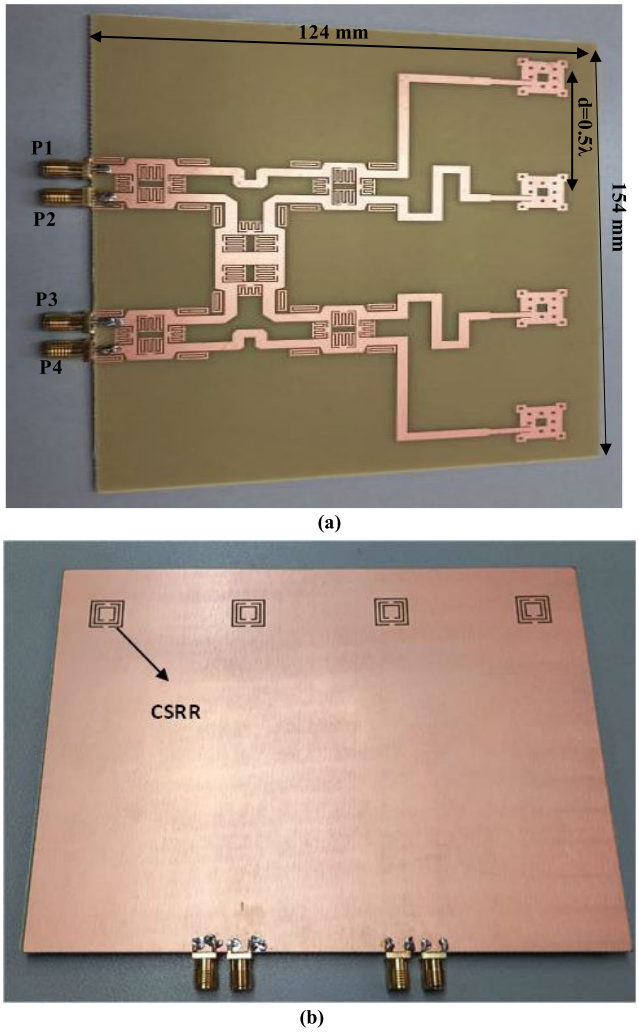


**FIGURE 18. Compact structure of the SAA, the spacing between the antenna elements d = 0.5$\lambda$ (a) Top layer (b) Bottom layer.**

achieved by the excitation of input ports P1, P2, P3, and P4, respectively. Based on the radiation patterns observed in Fig. 16(a), the direction of the main beam was attained at −8° and +8° by the excitation of P1 and P4, respectively. In Fig. 16(b), when input P2 and P3 are excited, the direction of the main beam is achieved at −23° and +23°, respectively.

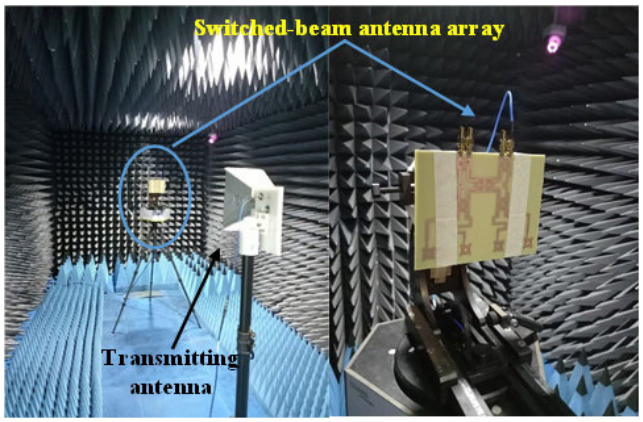


**FIGURE 19.** Setup for the radiation pattern measurement process.

This linear antenna array with $d = 0.7\lambda$ spacing has HPBW of 17.1°, 18.6°, 18.7°, and 17.1° when input ports P1, P2, P3, and P4 of BM are excited, respectively.

Table 4 shows the comparison of the simulated pattern results and the gain according to the spacing between the antenna elements ($d$). It is understood from the simulated results of the radiation pattern and comparison table that the grating lobe and the gain are reduced while decreasing the spacing between antenna components. The grating lobes and gain are raised, while the distance between the antenna is increased to $0.7\lambda$. The HPBW is more for $d = 0.3\lambda$. It is understood from the simulated results of the radiation pattern that there is variation in the main beam angle by decreasing/increasing the spacing between antenna elements from $0.5\lambda$. These radiation pattern studies show that the BM connected with the antenna has successfully generated four beams in four different directions.

From all these results, four MTM antennas based on CMSFA with CSRR etched in the ground plane connected to MTM-BM and the spacing between the antenna elements is $0.5\lambda$ were selected for fabrication. This structure shows the better gain and acceptable level of grating lobes are provided. The main purpose of fabrication is to validate our simulation result and analyse the switching of the beam in four different directions.

### B. LINEAR ANTENNA ARRAY (1 × 4) WITH BUTLER MATRIX FABRICATION AND CHARACTERIZATION

The planar bi-layer implementation of the linear antenna array with BM is performed by the combination of the designed MTM antenna in the article [15] and MTM based BM in section II-B at the center frequency of 3.5GHz. The hybrid implementation of the SAA is illustrated in Fig. 17. It can be seen in Fig. 17 that we have used the RF coaxial cables of 10cm to make the connection between the antenna and the BM, and the spacing between the antenna elements is $0.5\lambda$. However, this design is not applicable for the implementation in 5G applications because of its size and extra losses induced by the SMA transitions and coaxial cables. For us to make the design practical in 5G applications, the

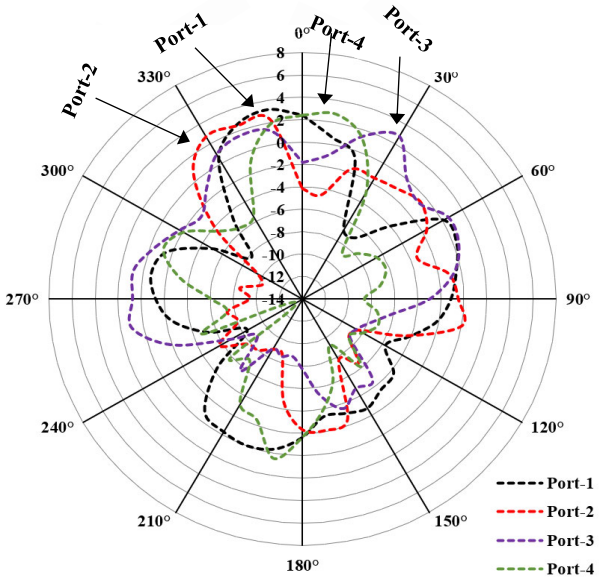


**FIGURE 20.** Radiation pattern of hybrid implementation of the SAA structure as shown previously in Fig.17.

design has to be more compact. Therefore, all components are fabricated on a single FR4 PCB substrate sharing a common ground plane. This can be observed in Fig. 18. With this compact design, the SAA has a total surface area of 124mm × 154mm. The radiation pattern measurements of the fabricated SAA are then performed in the anechoic chamber using Rohde & Schwarz ZVL vector network analyzer (VNA) and horn antenna shown in the measurement setup Fig. 19. Although there was some inconsistency noticed with the measured radiation pattern results from both SAA designs, they are minor enough for them to be a good match. The discrepancies may be due to extra losses and phase shifts prompted by the cables and connectors. The radiation pattern results of Fig. 17 are shown in Fig. 20. From now onwards, discussions relating to the results will be based on the compact structure of the SAA shown in Fig. 18.

## IV. RESULTS AND DISCUSSION

Fig. 21(a-b) shows the simulated and measured results of the radiation pattern of a linear 1 × 4 antenna array with a spacing of $0.5\lambda$ when P1, P2, P3, and P4 of the BM are excited. The simulation results were discussed in the already previous section, so now onwards, the discussion is related to the measured results. When P1 or P4 were excited, a gain of 4.8dB or 6.1dB was achieved, respectively. Meanwhile, the gain was 5dB and 5.1dB for P2 and P3 excitation, respectively. However, according to which input was excited, the peak of the beam rotates.

As seen in Fig. 21, when P1 was fed with a signal, the main beam steered to −15°. Meanwhile, the direction of maximum radiation was attained at −40°, as the signal was fed into P2. Based on Fig. 21, for the P3 excitation, the main beam steers to +45°. When Port-4 was excited, the direction of the main beam altered to +15°.

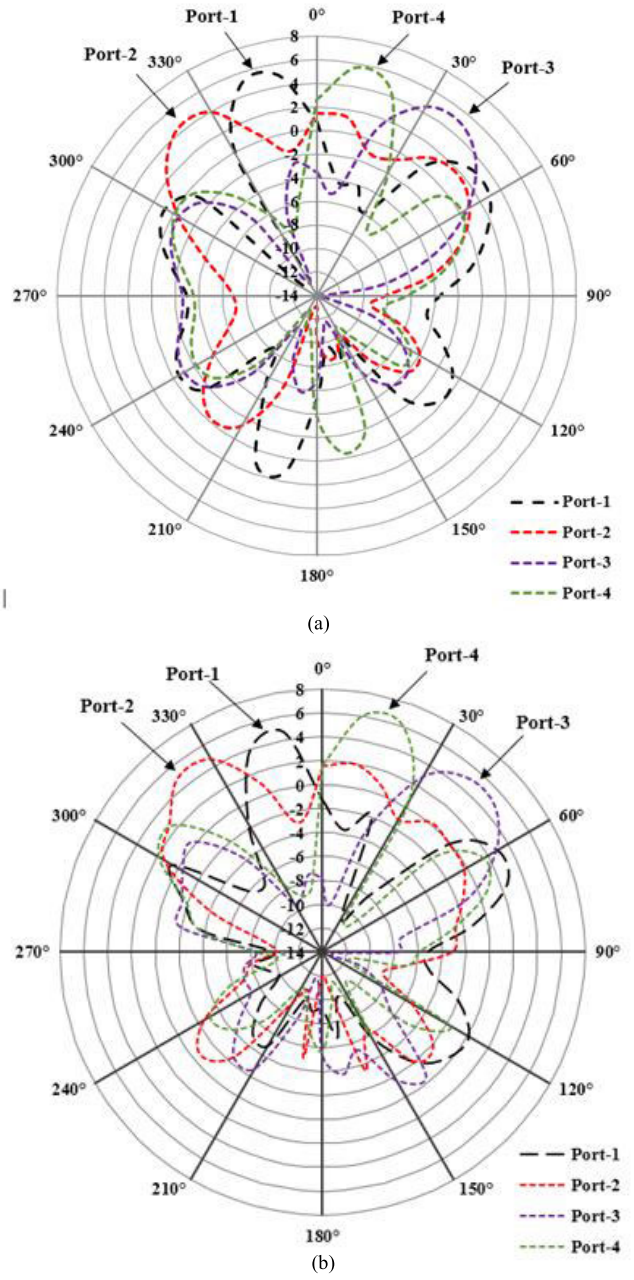


**FIGURE 21.** Radiation pattern results of linear 1×4 antenna array with a spacing of 0.5$\lambda$, when each input port of BM is excited (a) Simulated and (b) Measured result, respectively.

**TABLE 5.** Comparison of the simulated and measured radiation pattern results of linear 1 × 4 antenna array with a spacing of 0.5 $\lambda$.

| Port | Gain (dB) | | Main beam direction | |
|---|---|---|---|---|
| | Measured | Simulated | Measured | Simulated |
| Port-1 | 4.8 | 5.23 | -15° | -15° |
| Port-2 | 5 | 4.4 | -40° | -40° |
| Port-3 | 5.1 | 5.1 | +45° | +40° |
| Port-4 | 6.1 | 5.77 | +15° | +15° |

Table 5 shows the comparison of the simulated and measured radiation pattern results of a linear 1 × 4 antenna array with a spacing of 0.5$\lambda$. It can be seen from Table 5 that at the 3.5GHz operating frequency, the simulated and measured radiation pattern results for all the ports have a very good agreement. The Fig.22 illustrates the simulated and measured gains between the frequency range of 3-4GHz for the excitation of Port-1. It can be concluded that half of the semi-sphere ($-45° < \theta < +45°$) is scanned with a four-element MTM antenna array fed by the proposed BM circuit, with a maximum gain ranging between 4.8dB and 6.1dB. These radiation pattern studies have shown that the BM connected with the antenna has successfully generated four beams in different directions.

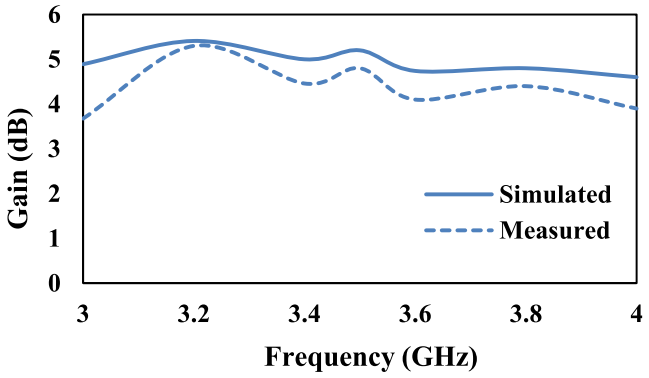


**FIGURE 22.** Gain stability of antenna array throughout the 3-4GHz frequency band.

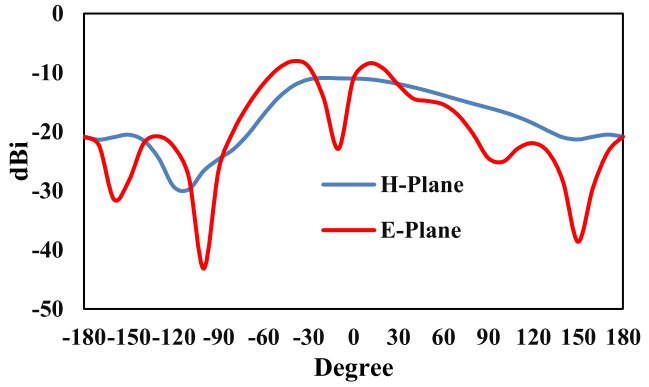


**FIGURE 23.** Cross-polarization studies for the E- & H-plane of the MTM based linear 1×4 antenna array.

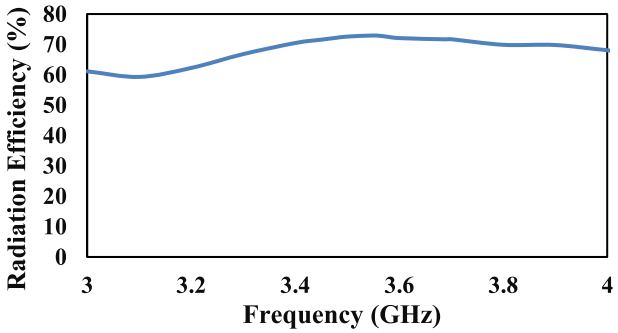


**FIGURE 24.** Radiation efficiency of proposed antenna array.

**TABLE 6.** Comparison between proposed SAA and existing antenna array system.

| Ref. | Operating Frequency (GHz) | Main Beam Angle (deg) | Beamwidth (deg) | Peak Gain (dB) | Bandwidth (MHz) | Substrate | Size | Structure |
|---|---|---|---|---|---|---|---|---|
| [26] | 1.96 | -39, -17, 9, 31 | 23, 27 | 9 | 100 | FR4 | 2.16 $\lambda_o \times 0.54\lambda_o$ | Planar |
| [27] | 2.4 | ± 20, ± 40 | 35.6,40.3, 39.8, 33.8 | 3.94 - 6.11 | 100 | FR4 | $2.25\lambda_o \times 2.1\lambda_o$ | Non-Planar |
| [28] | 2.4 | ± 12, −39, +37 | 20.7, 27, 26.3, 21.3 | 7.9 | 400 | Roger 4003C | $1.6\lambda_o \times 2.4\lambda_o$ | Planar |
| [18] | 3.5 | ±15, ±35 | 23,27,26,23 | 6.39 - 8.77 | 700 | Rogers 3003 | $1.8\lambda_o \times 1.6\lambda_o$ | Planar |
| [29] | 3.6 | - | - | 11.2 | 600 | Roger RT5880 | $2.47\lambda_o \times 3.5\lambda_o$ | Planar |
| [This Work] | 3.5 | -40, -15, +15, +45 | 22.3, 31.7 33.7, 23.6 | 4.8-6.1 | 550 | FR4 | 1.44 $\lambda_o \times 1.79\lambda_o$ | Planar |

Fig. 23 illustrates the cross-polarization studies for the E & H Plane of the MTM based linear 1 × 4 antenna array, respectively. According to Fig. 23, MTM based array antenna exhibits excellent isolation with a value less than −10dB for E- and H-plane.

The Fig 24 shows the radiation efficiency of the proposed MTM based antenna array, which shows an efficiency more than 70%. The single-element antenna is designed using FR4 substrate and its gain is nearly 2dBi. So, the first reason that the antenna array exhibits a low gain of around 5.5dBi is due to the lossy FR4 substrate, and another reason is the transmission-line loss between the antenna and feed network. The gain is further improved to 6.6dBi by keeping the antenna elements spacing of $0.7\lambda$ while realizing the array.

## V. COMPARISON TABLE

Table 6 shows the comparison between the proposed SAA and existing antenna array systems. The articles [26] and [27] in Table 5 attempt to improve the gain but suffer from narrow bandwidth. On the other hand, the articles in [18], [28], and [29] are fabricated on high-end Roger's substrates, providing an advantage of higher gain and wider bandwidth. However, none of the articles have covered the hemisphere's angle for radiation pattern coverage apart from the proposed design presented in this work. The proposed design not only enhances the overall bandwidth and gain, but also leads to a relatively smaller size as compared to other designs [18], [28], [29]. Additionally, it utilizes a low-cost substrate. Both the article [18] and the proposed design have almost similar results in terms of gain, bandwidth, and size, but the proposed SAA offers better coverage and uses low-cost materials, which makes it a unique choice for the upcoming 5G systems. Furthermore, article [18] has not validated their proposed design by fabricating the antenna array system. The gain of the proposed design can be further improved by using high-end substrates like Rogers. The results indicate that the proposed SAA is an excellent candidate for 5G application.

## VI. CONCLUSION

In this research article, MTM based switched-beam antenna array (SAA) was designed, simulated, and measured. More explicitly, the innovation relates to a compact Butler Matrix (BM) with an enhanced bandwidth intended to be used as a beamforming network (BFN) for SAA using an MTM structure. The proposed BM was implemented on a single FR4 substrate ($\varepsilon_r = 4.3$ and $h = 1.6$ mm) by integrating four compact 3dB BLCs, one 0dB crossover, and two 45° phase-shifters using the MTM-TL structure. The implementation of the MTM-TL structure provided a more compact system, enhanced the bandwidth, and improved the performance parameters. The proposed BLC operated in the frequency range of 2.87GHz - 4.17GHz with a coupling factor of 3 ±1dB and a phase difference of 88° between the output ports. The crossover was implemented by cascading two BLCs. The proposed BLC demonstrated a high fractional bandwidth of up to 40.2% and has a good profile that is 54% less in size than the conventional BLC design. The MTM-BM BFN measured results show excellent return-loss, isolation-loss, and insertion-loss, which cover the frequency range of 3.2GHz to 3.75GHz. The proposed BM achieves −45°, +135°, −135°, and +45° phase difference between the output ports with a maximum average phase-error of ±5°. This proposed BM is suitable to be integrated with the MTM antenna to construct a 5G SAA system.

The SAA has been developed by integrating MTM based BM and linear 1 × 4 MTM antenna on a single FR4 substrate to analyze the switching of the beam in the desired directions. The MTM antenna's radiating patch is based on the combined Minkowski- Sierpinski carpet fractal structure, and the ground plane of the antenna is etched with a complementary split-ring resonator (CSRR). The analysis of SAA has been done by varying the spacing between the four MTM antennas to identify the variation in main beam direction, gain, and grating lobe. The measured gain achieved by the $0.5\lambda$ spaced four linear MTM antenna connected to MTM BM is in the range of 4.8-6.1dB, when each input port of

the BM is excited. The radiation pattern results show that the main beam of SAA is directed in four different directions (−40°, −15°, +15°, +45°) based on the excitation of MTM BM input ports. The overall results of the SAA system show the beam-steering capabilities of the proposed design, which is the core requirement of the upcoming 5G wireless systems. So, it is envisioned that the proposed SAA system design can become a strong candidate for the upcoming 5G applications.

## REFERENCES

[1] J. G. Andrews, S. Buzzi, W. Choi, S. V. Hanly, A. Lozano, A. C. K. Soong, and J. C. Zhang, "What will 5G be?" *IEEE J. Sel. Areas Commun.*, vol. 32, no. 6, pp. 1065–1082, Jun. 2014, doi: 10.1109/JSAC.2014.2328098.

[2] T. S. Rappaport, S. Sun, R. Mayzus, H. Zhao, Y. Azar, K. Wang, G. N. Wong, J. K. Schulz, M. Samimi, and F. Gutierrez, "Millimeter wave mobile communications for 5G cellular: It will work!" *IEEE Access*, vol. 1, pp. 335–349, 2013, doi: 10.1109/ACCESS.2013.2260813.

[3] D. Muirhead, M. A. Imran, and K. Arshad, "A survey of the challenges, opportunities and use of multiple antennas in current and future 5G small cell base stations," *IEEE Access*, vol. 4, pp. 2952–2964, 2016, doi: 10.1109/ACCESS.2016.2569483.

[4] M. Agiwal, A. Roy, and N. Saxena, "Next generation 5G wireless networks: A comprehensive survey," *IEEE Commun. Surveys Tuts.*, vol. 18, no. 3, pp. 1617–1655, 3rd Quart., 2016, doi: 10.1109/COMST.2016.2532458.

[5] T. S. Rappaport, Y. Xing, O. Kanhere, S. Ju, A. Madanayake, S. Mandal, A. Alkhateeb, and G. C. Trichopoulos, "Wireless communications and applications above 100 GHz: Opportunities and challenges for 6G and beyond," *IEEE Access*, vol. 7, pp. 78729–78757, 2019, doi: 10.1109/ACCESS.2019.2921522.

[6] *Study on Implications of 5G Deployment on Future Business Models*. Accessed: Oct. 8, 2018. [Online]. Available: https://berec.europa.eu/eng/document_register/subject_matter/berec/reports/8008-study-on-implications-of-5g-deployment-on-future-business-models

[7] K. Shafique, B. A. Khawaja, F. Sabir, S. Qazi, and M. Mustaqim, "Internet of Things (IoT) for next-generation smart systems: A review of current challenges, future trends and prospects for emerging 5G-IoT scenarios," *IEEE Access*, vol. 8, pp. 23022–23040, 2020, doi: 10.1109/ACCESS.2020.2970118.

[8] C. Deng, D. Liu, B. Yektakhah, and K. Sarabandi, "Series-fed beam-steerable millimeter-wave antenna design with wide spatial coverage for 5G mobile terminals," *IEEE Trans. Antennas Propag.*, vol. 68, no. 5, pp. 3366–3376, May 2020.

[9] R. Xu and Z. N. Chen, "A compact beamsteering metasurface lens array antenna with low-cost phased array," *IEEE Trans. Antennas Propag.*, vol. 69, no. 4, pp. 1992–2002, Apr. 2021.

[10] D. Minoli and B. Occhiogrosso, "Practical aspects for the integration of 5G networks and IoT applications in smart cities environments," *Wireless Commun. Mobile Comput.*, vol. 2019, pp. 1–30, Aug. 2019. Accessed: Jan. 18, 2021. [Online]. Available: https://www.hindawi.com/journals/wcmc/2019/5710834/

[11] P. Pirinen, H. Pennanen, A. Pouttu, T. Tuovinen, N. Tervo, P. Luoto, A. Roivainen, A. Pärssinen, and M. Latva-aho, "RF driven 5G system design for centimeter waves," *Wireless Commun. Mobile Comput.*, vol. 2018, pp. 1–9, May 2018. Accessed: Jan. 5, 2021. [Online]. Available: https://www.hindawi.com/journals/wcmc/2018/7852896/

[12] O. E. Ayach, S. Rajagopal, S. Abu-Surra, Z. Pi, and R. W. Heath Jr., "Spatially sparse precoding in millimeter wave MIMO systems," *IEEE Trans. Wireless Commun.*, vol. 13, no. 3, pp. 1499–1513, Mar. 2014, doi: 10.1109/TWC.2014.011714.130846.

[13] R. Méndez-Rial, C. Rusu, N. González-Prelcic, A. Alkhateeb, and R. W. Heath Jr., "Hybrid MIMO architectures for millimeter wave communications: Phase shifters or switches?" *IEEE Access*, vol. 4, pp. 247–267, 2016, doi: 10.1109/ACCESS.2015.2514261.

[14] W. Nie, Y. Fan, S. Luo, and Y. Guo, "A switched-beam microstrip antenna array with miniaturized Butler matrix network," *Microw. Opt. Technol. Lett.*, vol. 57, no. 4, pp. 841–845, Apr. 2015, doi: 10.1002/mop.28972.

[15] A. K. Vallappil, M. K. A. Rahim, B. A. Khawaja, M. N. Iqbal, N. A. Murad, M. M. Gajibo, L. O. Nur, and B. S. Nugroho, "Complementary split-ring resonator and strip-gap based metamaterial fractal antenna with miniature size and enhanced bandwidth for 5G applications," *J. Electromagn. Waves Appl.*, vol. 36, no. 6, pp. 787–803, Sep. 2021, doi: 10.1080/09205071.2021.1983878.

[16] A. Vallappil, B. Khawaja, M. Rahim, M. Iqbal, H. Chattha, and M. Ali, "A compact triple-band UWB inverted triangular antenna with dual-notch band characteristics using SSRR metamaterial structure for use in next-generation wireless systems," *Fractal Fractional*, vol. 6, no. 8, p. 422, Jul. 2022, doi: 10.3390/fractalfract6080422.

[17] A. K. Vallappil, M. K. A. Rahim, B. A. Khawaja, and N. A. Murad, "Metamaterial Sierpinski carpet antenna with cross-slot superstrate for 5G applications," in *Proc. IEEE Int. Symp. Antennas Propag. USNC-URSI Radio Sci. Meeting (APS/URSI)*, Dec. 2021, pp. 1964–1965, doi: 10.1109/APS/URSI47566.2021.9704730.

[18] N. T. Tokan, "Array antenna feeding network design for 5G MIMO applications," *Electrica*, vol. 19, no. 2, pp. 120–127, Jul. 2019.

[19] J. Butler, "Beam-forming matrix simplifies design of electronically scanned antennas," *Electron. Des.*, vol. 12, pp. 170–173, Dec. 1961.

[20] H. Moody, "The systematic design of the Butler matrix," *IEEE Trans. Antennas Propag.*, vol. AP-12, no. 6, pp. 786–788, Nov. 1964, doi: 10.1109/TAP.1964.1138319.

[21] G. A. Adamidis, I. O. Vardiambasis, M. P. Ioannidou, and T. N. Kapetanakis, "Design and implementation of single-layer 4 × 4 and 8 × 8 Butler matrices for multibeam antenna arrays," *Int. J. Antennas Propag.*, vol. 2019, pp. 1–12, Mar. 2019. Accessed: Sep. 22, 2020. [Online]. Available: https://www.hindawi.com/journals/ijap/2019/1645281/

[22] O. Abu Safia, M. Nedil, M. C. E. Yagoub, and W. Yusuf, "Optically transparent compact 4×4 Butler matrix for Wi-Fi applications," *Prog. Electromagn. Res. Lett.*, vol. 58, pp. 119–124, 2016, doi: 10.2528/PIERL15101004.

[23] A. K. Vallappil, M. K. A. Rahim, B. A. Khawaja, and M. Aminu-Baba, "Metamaterial based compact branch-line coupler with enhanced bandwidth for use in 5G applications," *Appl. Comput. Electromagn. Soc. J.*, vol. 35, pp. 700–708, Jun. 2020.

[24] D. M. Pozar, *Microwave Engineering*, 3rd ed. Wiley, 2005.

[25] S. Sahin, N. K. Nahar, and K. Sertel, "A simplified Nicolson–Ross–Weir method for material characterization using single-port measurements," *IEEE Trans. Terahertz Sci. Technol.*, vol. 10, no. 4, pp. 404–410, Jul. 2020, doi: 10.1109/TTHZ.2020.2980442.

[26] Y.-J. Kim, Y.-B. Kim, H.-J. Dong, Y. S. Cho, and H. L. Lee, "Compact switched-beam array antenna with a Butler matrix and a folded ground structure," *Electronics*, vol. 9, no. 1, p. 2, Dec. 2019.

[27] F. Y. Zulkifli, N. Chasanah, Basari, and E. T. Rahardjo, "Design of Butler matrix integrated with antenna array for beam forming," in *Proc. Int. Symp. Antennas Propag. (ISAP)*, Nov. 2015, pp. 1–4.

[28] T. D. Bui, M. T. Le, and Q. C. Nguyen, "Electronically steerable antenna array for indoor positioning system," *J. Electromagn. Waves Appl.*, vol. 33, no. 7, pp. 838–852, May 2019.

[29] A. Khairy, A. Elboushi, A. A. Shaalan, and M. F. Ahmed, "Analysis and design of sub-6 beam steerable antenna array using meta-material loaded Vivaldi elements," *Anal. Integr. Circuits Signal Process.*, vol. 115, no. 1, pp. 159–168, Apr. 2023.

**ARSHAD KARIMBU VALLAPPIL** received the B.Tech. degree in electronics and communication engineering from the University of Calicut, Kerala, India, in 2009, the M.Tech. degree in electronics engineering from Pondicherry University, Puducherry, India, in 2013, and the Ph.D. degree in electrical from Universiti Teknologi Malaysia, Malaysia, in 2021. He is currently with the Institute of Space Sciences, Barcelona, Spain. His research interests include RF and microwave systems, antenna arrays, beamforming networks, meta-materials, and meta-surfaces.

**MOHAMAD KAMAL A. RAHIM** (Senior Member, IEEE) was born in Alor Setar, Kedah, Malaysia, in 1964. He received the B.Eng. degree in electrical and electronic engineering from the University of Strathclyde, U.K., in 1987, the master's degree in engineering from the University of New South Wales, Australia, in 1992, and the Ph.D. degree in wideband active antenna from the University of Birmingham, U.K., in 2003. From 1992 to 1999, he was a Lecturer with the Faculty of Electrical Engineering, Universiti Teknologi Malaysia. He was a Senior Lecturer with the Department of Communication Engineering, from 2005 to 2007. He is currently a Professor with Universiti Teknologi Malaysia. His research interests include the design of active and passive antennas, dielectric resonator antennas, microstrip antennas, reflectarray antennas, electromagnetic bandgap, artificial magnetic conductors, left-handed metamaterials, and computer-aided design for antennas.

**BILAL A. KHAWAJA** (Senior Member, IEEE) received the B.S. degree in computer engineering from the Sir Syed University of Engineering and Technology, Karachi, Pakistan, in 2002, the M.Sc. degree in communication engineering and signal processing from the University of Plymouth, Plymouth, U.K., in 2005, and the Ph.D. degree in electrical engineering from the University of Bristol, Bristol, U.K., in 2010. From 2010 to 2016, he was an Assistant Professor with the Electronics and Power Engineering Department, P. N. Engineering College, National University of Science and Technology (NUST), Karachi. In 2015, he was a Visiting Postdoctoral Researcher with the Lightwave Systems Research Laboratory, Queen's University, Kingston, Canada, involved in the Natural Sciences and Engineering Research Council (NSERC)-Canada CREATE Next Generation Optical Network (NGON) Project on the characterization and measurements of 25GHz RF signal generation optical comb sources. He is currently an Associate Professor with the Department of Electrical Engineering, Faculty of Engineering, Islamic University of Madinah, Madinah, Saudi Arabia. He has authored and coauthored several journals and IEEE proceeding publications. His current research interests include antenna/antenna array design for the 5G/the IoT/UAVs/FANETs/Wi-Fi systems/UWB wireless body area networks, wireless sensor networks, and millimeter-wave frequency bands. He is also actively working in the area of metamaterials/metasurfaces and the use of artificial intelligence (AI) and blockchain technology in the 5G/6G/next-generation wireless systems.

**MUHAMMAD NAEEM IQBAL** was born in Mangla, Pakistan, in 1987. He received the bachelor's and master's degrees in electrical engineering from the National University of Sciences and Technology, Pakistan, in 2009 and 2013, respectively, and the Ph.D. degree in electrical engineering from Universiti Teknologi Malaysia. His research interests include the transmitarray antennas, reflectarray antennas, beam forming, and polarization converters.